Wing 3D Reconstruction by Constraining the Bundle Adjustment with Mechanical Limitations

Quentin Demoulin, Adrian Basarab, Denis Kouamé, Jean-Yves Tourneret

Wing 3D Reconstruction by Constraining the Bundle Adjustment with Mechanical Limitations

Quentin Demoulin*†, François Lefebvre-Albaret*, Adrian Basarab‡, Denis Kouamé‡ and Jean-Yves Tourneret†
*Airbus, 316 route de Bayonne, 31060 Toulouse, France
†IRIT/ENSEEIHT/Tésa, University of Toulouse, 31071 Toulouse, France
‡IRIT UMR CNRS 5505, University of Toulouse, Université Paul Sabatier, CNRS, France
Email: quentin.demoulin@airbus.com

***Abstract*—The estimation of wing deformation is part of the certification of an aircraft. Wing deformation can be obtained from 3D reconstructions based on conventional multi-view photogrammetry. However, 3D reconstructions are generally degraded by the variable flight environments that degrade the quality of 2D images. This paper addresses this issue by taking benefit from *a priori* knowledge of the wing mechanical behaviour. Specifically, mechanical limits are considered to regularize the bundle adjustment within the photogrammetry reconstruction. The performance of the proposed approach is evaluated on a real case, using data acquired on an aircraft A350-900.**

***Index Terms*—Bundle adjustment, optimization under constraints, wing deformations, mechanical limits.**

I. Introduction

Long before the first flight of an aircraft, manufacturers are able to predict its mechanical behavior in various scenarii depending for instance on the aircraft weight, speed or angle of attack, based on accurate theoretical models. As part of aircraft certification procedure, these models have to be validated and refined through in-flight estimation of wing deformations. To this end, we introduce in this paper a new multiple-view photogrammetry method that reconstructs the wing 3D shape in flight from the observations, *i.e.*, 2D pictures of cameras installed inside the aircraft. Similarly to most standard photogrammetry methods, the proposed approach is based on Bundle Adjustment (BA), a classical method that simultaneously estimates camera positions and surrounding 3D scene [1, p. 434]. BA was initially introduced for photogrammetry reconstructions, and has been upgraded and popularized in robotics and computer applications, with structure from motion (SfM) [2], [3] or full simultaneous localization and mapping (SLAM) [4] techniques.

BA is an iterative optimization algorithm that aims at minimizing a non convex and non-linear cost function. Therefore, one cannot guarantee its convergence to a global minimum, and the choice of the initial conditions is crucial in practical applications. Consequently, the application of photogrammetry to 3D wing reconstruction in flight is a very challenging problem. First, camera positions suffer from strong installation constraints, given that today they can only be located on the rear vertical stabilizer of the aircraft and on the aircraft windows. With this setup, the wing end is observed under very low angles, directly impacting the accuracy of point detection in images. Besides, the distance between cameras is also restricted to guaranty covering in views of the wing, i.e., almost 15m separate for a 30m long wing. Second, highly varying environment strongly affects the observations: the whole aircraft itself is deforming and vibrating, and the 2D images are subject to luminosity changes, potential reflections and shadows. As a consequence, observation uncertainties prevent the standard BA method from obtaining accurate 3D wing reconstructions.

During the previous years, various constrained optimization methods were developed to improve the performance of the classical BA approach, taking benefit of prior knowledge about the scene or system to reconstruct. In [5], [6], prior knowledge of point coplanarity between neighboring points or information about their positions constructed from a Digital Terrain Model (DTM) are introduced in the BA as constraints on the unknown parameters. Similarly, information red camera positions acquired from the Global Positioning System (GPS) or Inertial Measurement Units (IMUs) are introduced in the BA as constraints for the camera parameters in [2], [7], [8]. In [9], improvements on SLAM accuracy and robustness is achieved using GPS together with DTM as priors. Finally, knowledge about 3D structure models is introduced in model-assisted BA to impose proximity between reconstructed 3D points and a reference model [10], [11].

In the case of wing deformation estimation, one cannot introduce directly prior knowledge on the wing structure model in the BA reconstruction, since the main objective is to practically evaluate this model. Instead, we propose in this work to use prior knowledge resulting from wing mechanical limits, beyond which the wing would break. The major contribution of this paper is to redefine the BA reconstruction problem such that it efficiently constrains the 3D points to respect these mechanical limits, by introducing suitable regularization terms in the BA cost function.

The remainder of the paper is organized as follows. Section II introduces the proposed model for wing deformations. Section III reminds the principle of BA for 3D wing reconstruction. The proposed BA cost function, defined as the combination of BA and wing limits, is presented in Section IV. Experimental results are shown in Section V. Conclusions and perspectives are reported in Section VI.

The authors would like to thank Airbus for funding and support.

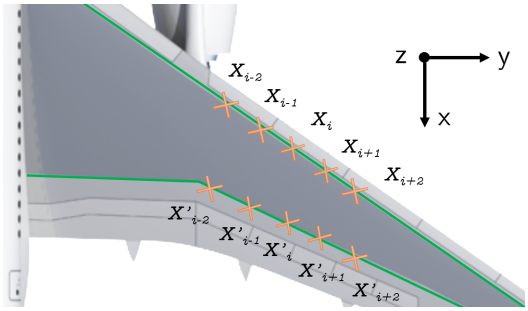

Fig. 1. Node illustration on the aircraft wing.

II. Wing deformation model

Although challenging because of the specific flight test environment, wing deformation estimation can rely on a range of prior information. On the image processing side, views in flight are always the same, facilitating the detection and tracking of points of interest. The latter is also facilitated by the presence of two black lines along the wing span, represented in Fig. 1 as green lines, allowing one to define a set of nodes to track. Wing mechanical properties enable the use of even richer prior information, since wings are build on theoretical models using Finite Element Models (FEM). In addition to geometry scales, predicted wing deformations are thus available for any flight configuration. However, these predictions cannot be used in the particular application addressed herein. More precisely, theoretical deformation models cannot be used to robustify 3D wing reconstructions, because these reconstructions are supposed to validate (or not) these models. Instead, this work aims at exploiting the mechanical limits derived from the FEM. Specifically, limit conditions corresponding to situations where the structure materials would break are considered. We assume that these extreme cases, corresponding to the wing shattering, will not occur during tests. This work defines maximum and minimum deformations as constraints in the BA algorithm.

Consider N 3D-points used for wing reconstruction denoted as $\boldsymbol{X}^i$ for $i = 1, ..., N$, and denote as $\boldsymbol{X}^i = (x^i, y^i, z^i)$ the ith deformation point, using axes as shown in Fig. 1. This paper proposes to use the following set of limits

i. Volume limits: each point has a specific maximum volume (sphere, ellipsoid, or some volume defined according to the FEM data).
ii. Bending limits: $\forall i, \exists (b^i_{\min}, b^i_{\max})$, such that the bending $\dfrac{\partial^2 z^i}{\partial y^2}$ ranges in $[b^i_{\min}, b^i_{\max}]$.
iii. Torsion limits: $\forall i, \exists (t^i_{\min}, t^i_{\max})$, such that the torsion $\dfrac{\partial^2 z^i}{\partial x \partial y}$ ranges in $[t^i_{\min}, t^i_{\max}]$.
iv. Relative elongation limits: $\forall i, \exists \epsilon^i$, such that

$$\frac{d(\boldsymbol{X}^i, \boldsymbol{X}^{i-1}) - d_0(\boldsymbol{X}^i, \boldsymbol{X}^{i-1})}{d_0(\boldsymbol{X}^i, \boldsymbol{X}^{i-1})} < \epsilon^i \tag{1}$$

where $d(\boldsymbol{X}^i, \boldsymbol{X}^{i-1})$ is the Euclidean distance between points $\boldsymbol{X}^i$ and $\boldsymbol{X}^{i-1}$ in the (x, y) plane, and $d_0(\boldsymbol{X}^i, \boldsymbol{X}^{i-1})$ is the initial distance before deformation.

To integrate these limits in the wing reconstruction process, we make the assumption that the limits are locally valid, which allows their definition using finite differences on a set of nodes in the (x, y) plane. Considering the node $\boldsymbol{X}^i$ and its neighborhood $(\boldsymbol{X}^{i-2}, \ldots, \boldsymbol{X}^{i+2}, \boldsymbol{X}'^{i-2}, \ldots, \boldsymbol{X}'^{i+2})$, detected on the wing lines as illustrated in Fig. 1 ($\boldsymbol{X}^i$ and $\boldsymbol{X}'^i$ are on the same ith wing section (i.e., along the same coordinate y axis), one can define a set of C constraints $(g_k)_{k=0,\ldots,C}$.

i. Volume constraint is expressed as 3D points having a limited displacements in the (x, y) plane, leading to:

$$g_0(\boldsymbol{X}^i) = \sqrt{(\tilde{x}^i - x^i_{\text{init}})^2 + (\tilde{y}^i - y^i_{\text{init}})^2} - a < 0, \tag{2}$$

where a is the maximum radius, and $\boldsymbol{X}^i_{\text{init}}$ is the initial position of point i before deformation.

ii. Bending constraints: $\forall i, \exists (b_{\min}, b_{\max})$, such that

$$g_1(\boldsymbol{X}^i) = \frac{z_{i+1} - 2z_i + z_{i-1}}{(y_{i+1} - y_i)^2} - b^i_{\max} < 0, \tag{3}$$

$$g_2(\boldsymbol{X}^i) = b^i_{\min} - \frac{z_{i+1} - 2z_i + z_{i-1}}{(y_{i+1} - y_i)^2} < 0. \tag{4}$$

iii. Torsion constraints: The two nodes located in section $\#i$ are constrained by the adjacent section $\#(i-1)$, leading to $\forall i, \exists (t^i_{\min}, t^i_{\max})$ such that

$$g_3(\boldsymbol{X}^i) = \frac{z'_i - z'_{i-1} - z_i + z_{i-1}}{4(x'_i - x_i)(y_i - y_{i-1})} - t^i_{\max} < 0, \tag{5}$$

$$g_4(\boldsymbol{X}^i) = t^i_{\min} - \frac{z'_i - z'_{i-1} - z_i + z_{i-1}}{4(x'_i - x_i)(y_i - y_{i-1})} < 0. \tag{6}$$

iv. Relative elongation constraint: $\forall i, \exists \epsilon^i$, such that

$$g_5(\boldsymbol{X}^i) = \frac{d(\boldsymbol{X}^i, \boldsymbol{X}^{i-1}) - d_0(\boldsymbol{X}^i, \boldsymbol{X}^{i-1})}{d_0(\boldsymbol{X}^i, \boldsymbol{X}^{i-1})} - \epsilon^i < 0. \tag{7}$$

III. Bundle adjustment

BA is commonly used to recover 3D-point coordinates and camera parameters from 2D observations in more than 2 view photogrammetry systems. Let $\boldsymbol{\alpha}_j = (\boldsymbol{v}^j, \boldsymbol{t}_j)^T$ be the parameter vector of the jth camera, where $\boldsymbol{v}^j$ is the 3×1 rotation vector and $(\boldsymbol{t}_j)$ is the 3×1 translation vector. Given a set of M cameras and the N 3D-points $\boldsymbol{X}^i$, the algorithm seeks to minimize the distance between the projections of $\boldsymbol{X}^i$ on the jth camera for $j = 1, \ldots, M$, denoted as $\hat{\boldsymbol{x}}(\boldsymbol{\alpha}_j, \boldsymbol{X}^i)$, and the matching 2D points $(\boldsymbol{x}^i_j)$ from camera observations:

$$\underset{\boldsymbol{\alpha}_j, \boldsymbol{X}^i}{\arg\min} \sum_{i,j} \left[\boldsymbol{x}^i_j - \hat{\boldsymbol{x}}(\boldsymbol{\alpha}_j, \boldsymbol{X}^i)\right]^2, \tag{8}$$

where

$$\hat{\boldsymbol{x}}(\boldsymbol{\alpha}_j, \boldsymbol{X}^i) = \frac{1}{c^i_j} \boldsymbol{K}_j \boldsymbol{l}^i_j, \tag{9}$$

with $\boldsymbol{K}_j$ a 2×3 matrix of the intrinsic camera parameters, considered as known after system calibration, and

$$\boldsymbol{l}^i_j = (a^i_j, b^i_j, c^i_j)^T = \left[\boldsymbol{R}^T_j, -\boldsymbol{R}^T_j \boldsymbol{t}_j\right] \begin{pmatrix} \boldsymbol{X}^i \\ 1 \end{pmatrix}, \tag{10}$$

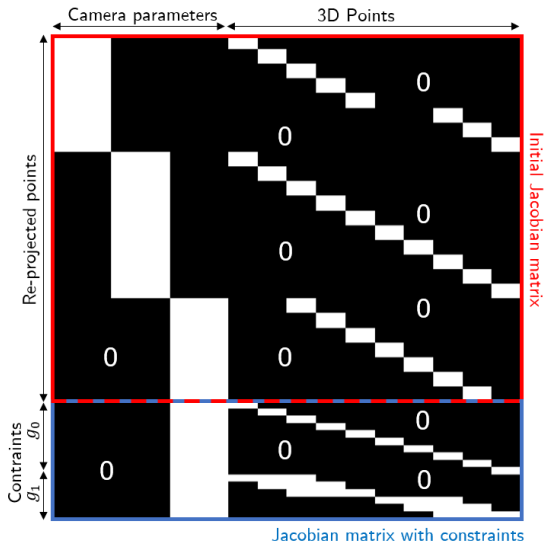

Fig. 2. Example of sparse bundle adjustment Jacobian matrix for 3 cameras and 10 points. The last rows represent the two first constraints g_0 and g_1 defined in Section II.

with $\boldsymbol{R}_j$ the rotation matrix formed using the Euler-Rodrigues formula [12], corresponding to a rotation of angle θ_j around the axis represented by the unit vector $\bar{\boldsymbol{v}}_j$, such that $\boldsymbol{v}_j = \theta \bar{\boldsymbol{v}}_j$. Note that one can also represent the rotations using the three Euler angles. However, the rotation vector is preferred here since it removes the ambiguity of rotation order, and enables a faster Python implementation.

The 3D reconstruction problem (8) is highly non-convex and non-linear. To solve it, one can consider using iterative methods such as Gauss-Newton or Levenberg Marquardt (see [6] or [1, p. 597]). These two methods use iterative steps from the initial guess to the optimum parameter using the Hessian matrix, approximated as $\boldsymbol{J}^T\boldsymbol{J}$, where $\boldsymbol{J}$ is the Jacobian matrix. The Jacobian matrix in BA has the interesting characteristic of being sparse, thus significantly fastening the optimization procedure. Indeed, each projected point depends only on the corresponding 3D point and on the camera, leading to:

$$\frac{\partial(\boldsymbol{x}_j^p - \hat{\boldsymbol{x}}(\boldsymbol{\alpha}_j, \boldsymbol{X}^p))^2}{\partial \boldsymbol{X}^q} = 0, \forall p \neq q, \forall j \in \{1, ..., M\} \quad (11)$$

$$\frac{\partial(\boldsymbol{x}_p^i - \hat{\boldsymbol{x}}(\boldsymbol{\alpha}_p, \boldsymbol{X}^i))^2}{\partial \boldsymbol{\alpha}_q} = 0, \forall p \neq q, \forall i \in \{1, ..., N\}. \quad (12)$$

Furthermore, some points may not be seen by some cameras, leading to additional empty lines in the Jacobian matrix. An example of Jacobian matrix used in BA is presented in Fig. 2, where the only non-zero elements are displayed in white.

IV. Constrained Bundle Adjustment

This section explains how to introduce the previously defined constraints in BA. In this work, because of camera motions during the flight, 3D coordinates of the points and cameras are estimated in a moving coordinate system, while the considered constraints are considered in the aircraft coordinate system. Therefore, an additional registration phase is required to transfer the points in the aircraft coordinate system. To perform this operation, the aircraft reference points are detected from the rear camera image, further used to estimate the transfer matrix $\boldsymbol{P}$ from the aircraft coordinate system to the camera system. Using the estimated parameters $\boldsymbol{\alpha}_r$ from the same camera, the points $\tilde{\boldsymbol{X}}^i$ are then registered as:

$$\tilde{\boldsymbol{X}}^i = \boldsymbol{P} \left[\boldsymbol{R}_r^T, -\boldsymbol{R}_r^T \boldsymbol{t}_r\right] \boldsymbol{X}^i, \quad (13)$$

where $\boldsymbol{R}_r$ and $\boldsymbol{t}_r$ are the parameters of the rth camera, as defined in Section III.

After the registration phase, the constraints introduced in Section II are expressed as regularization terms to penalize the objective function (8) [13, p. 564], defining the new following regularized optimization problem (called CBA hereafter):

$$\underset{\boldsymbol{\alpha_j}, \boldsymbol{X}^i}{\arg\min} \sum_{i,j} \left[\boldsymbol{x}_j^i - \hat{\boldsymbol{x}}(\boldsymbol{\alpha}_j, \boldsymbol{X}^i)\right]^2 + \sum_k \mu_k \left\{\sum_i \left[g_k^+(\boldsymbol{\alpha}_r, \tilde{\boldsymbol{X}}^i)\right]^2\right\}, \quad (14)$$

where μ_k are positive hyperparameters and $g_k^+(\boldsymbol{\alpha}_r, \tilde{\boldsymbol{X}}^i) = \max(0, g_k(\boldsymbol{\alpha}_r, \tilde{\boldsymbol{X}}^i))$, with g_k the kth constraint.

With this formulation, μ_k equals zero when the corresponding constraint is respected, and therefore this penalty does not impact the results. As explained previously, the optimization method used by BA is based on the Jacobian matrix, which requires the objective function to be differentiable. To enforce differentiability of (14), we use the *Courant-Beltrami* penalty function [13, p. 566], with a quadratic term on g_k^+, which also smooths this function. Finally, since the constraints are applied to specific point neighbourhoods, and depend only on the rear camera parameters, the sparsity of the Jacobian matrix is preserved, as shown by the example in Fig. 2, considering the derivative of each element of the projection error and constraints with respect to all camera and point parameters. Similarly to the classical BA problem, the sparsity of the Jacobian matrix significantly reduces the computational cost of the optimization algorithm. To further improve the computational cost of the optimization, this work proposes to use an analytical form of the Jacobian matrix (see [14] for details), instead of the usual approach that estimates it numerically by finite differences.

V. Experimental Results

Real data from a ground test was acquired on an Airbus A350-900 to evaluate the proposed method. To reproduce an installation similar to the one foreseen during flights, cross targets were installed on the wing surface to improve the accuracy of point detection in the images. Four 4K cameras were installed on the aircraft windows. The rear camera was simulated by a drone placed on the vertical stabilizer. Examples of images acquired by these cameras are displayed in Fig. 3. To clearly identify the points on which deformation constraints are applied, graduations were stuck on the two black lines every 30 cm, which will define the nodes of the proposed wing reconstruction.

(a) Camera 1 (b) Rear camera (c) Camera 3

Fig. 3. Examples of recorded views resulting from a test on ground with an Airbus A350-900.

After installation, a drone was used along with the software Agisoft Metashape [15] to perform a scan of the wing and initialize the camera and point positions. Finally, wing vibration was generated by manually shaking the wing tip of about 5 cm (the vertical motion amplitude was estimated using a scale board). As expected, the detection of graduations observed with low angles was less accurate compared to large angles (see wing tips in cameras 1 and 3 in Fig. 3). In addition, graduation detection was not possible in some images because of reflections on the wing (see camera 3 in Fig. 3).

The proposed constrained algorithm (CBA) was implemented in Python and compared to the classical unconstrained BA algorithm. The constrained optimization was performed using the least-squares "trust region reflective" method implemented in the Scipy library [16], benefiting from its capability to take a function to construct the Jacobian matrix as input. The mechanical limits $(a, b^i_{\max}, b^i_{\min})$ were estimated from data resulting from existing flight tests provided by Airbus. Penalization hyperparameters were set to $(\mu_0, \mu_1, \mu_2) = (10^4, 10^3, 10^4)$ by cross validation. Point and camera positions were extracted from a representative video of the moving wing, by running 30 frames through our algorithm. For comparison, we used unconstrained BA, BA with constrained volume, BA with constrained bending, and BA with both volume and bending constrains (respectively denoted as "BA", "CBA_V", "CBA_B" and "CBA_VB").

Fig. 4 shows that the camera estimation precision is enhanced using CBA_V and CBA_VB algorithms, as cameras were supposed to have negligible motions during the ground test. In particular, it can be observed that camera motions is reduced compared to BA. Furthermore, Fig. 5 shows that using the volume constraint significantly improves the estimation results, resulting into an amplitude of 5 cm at wing tip and of less than 1cm in the middle of the wing, which is consistent with our measurements using the scale board. On the contrary, using the bending constraint alone does not provide good estimation results. The distance between the wing reconstruction and the theoretical ground shape (computed using Cloud Compare [17]) displayed in Fig. 6 shows that the distance at the wing start is reduced using CBA_VB (of more than 0.2m compared to CBA_V). As a consequence, the combination of local volume and bending constraints improves the global estimation, as points at the wing start should be closer to the model, where it is more rigid, than at the end. Note that FEM

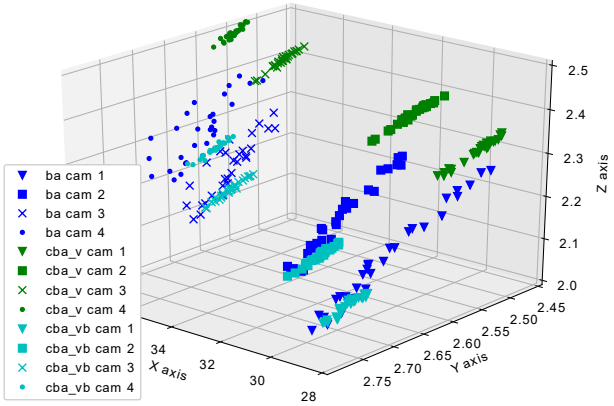

Fig. 4. Estimated motions (in meters) of the 4 cameras located on the aircraft windows versus time.

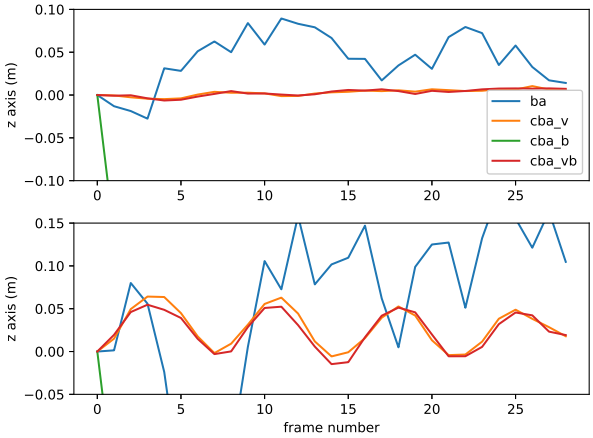

Fig. 5. Bending results at the middle of the wing (top) and at wing tip (bottom).

is only a model, which is is not supposed to perfectly fit the data. Thus, a deviation from this model is possible. Finally, estimation results versus time, illustrated in Fig. 7, suggest that the volume constraint is correctly respected and improves point position tracking, all points remaining close to their initial location in the (x, y) plan.

VI. Conclusions

This article proposed to introduce mechanical limits of an aircraft wing deformation into a bundle adjustment algorithm for 3D estimation using multi-view photogrammetry. For this

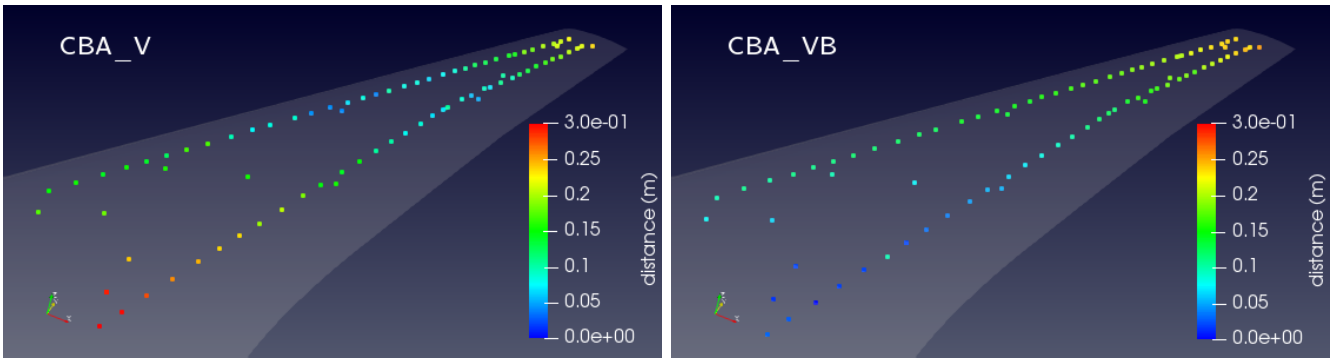

Fig. 6. Comparison of the distances between the reconstructed point cloud and the theoretical model of ground shape. (left) reconstruction using only volume constraint, (right) reconstruction using both volume and bending constraints.

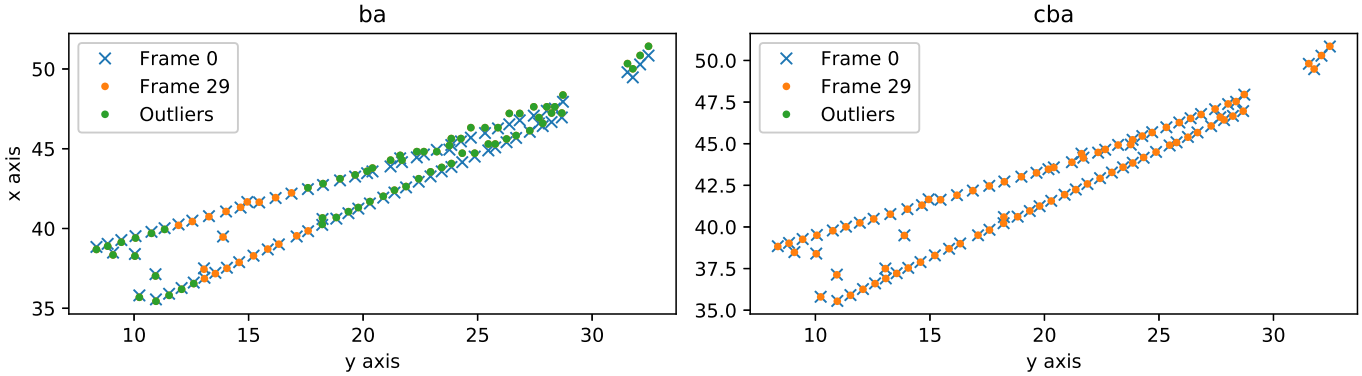

Fig. 7. Point reconstructions in the (x, y) plane for the first and last frames. (left) without the constraint, (right) with the volume and bending constraints. Some outliers not respecting the constraints can be observed in the last ba frame.

purpose, regularization terms were considered into the classical bundle adjustment method. The potential of the proposed method was demonstrated through realistic experiments conducted on images acquired on an aircraft located on the ground. The application of all the proposed constraints in flight is clearly an interesting prospect. Another area of improvement is to use weighted bundle adjustment to reduce the influence of wrong observations on the reconstruction. Finally, it would be interesting to study the hybridization of the proposed method with data from other sensors such as inertial units.

References

[1] R. Hartley and A. Zisserman, *Multiple View Geometry in Computer Vision*, Cambridge University Press, New York, NY, USA, 2004.

[2] D. Larnaout, V. Gay-Bellile, S. Bourgeois, and M. Dhome, "Vehicle 6-DoF localization based on SLAM constrained by GPS and digital elevation model information," in *Proc. Int. Conf Image Process. (ICIP)*, Melbourne, Australia, Sep. 2013.

[3] A. P. Bustos, T.-J. Chin, A. Eriksson, and I. Reid, "Visual SLAM: Why bundle adjust?," in *Proc. Int. Conf. on Robotics and Automation (ICRA)*, Montréal, Canada, May. 2019.

[4] V. Indelman, R. Roberts, and F. Dellaert, "Incremental light bundle adjustment for structure from motion and robotics," *Robotics and Autonomous Systems*, vol. 70, pp. 63–82, Aug. 2015.

[5] Y. Zhang, K. Hu, and R. Huang, "Bundle adjustment with additional constraints applied to imagery of the dunhuang wall paintings," *ISPRS Journal of Photogrammetry and Remote Sensing*, vol. 72, pp. 113–120, Aug. 2012.

[6] G. Briskin, A. Geva, E. Rivlin, and H. Rotstein, "Estimating pose and motion using bundle adjustment and digital elevation model constraints," *IEEE Trans. Aerosp. Electron. Syst.*, vol. 53, no. 4, pp. 1614–1624, Aug. 2017.

[7] B. Heiner and C. N. Taylor, "Creation of geo-referenced mosaics from MAV video and telemetry using constrained optimization bundle adjustment," in *Proc. Int. Conf. on Intelligent Robots and Systems*, St Louis, St Louis, USA, Oct. 2009.

[8] M. Lhuillier, "Incremental fusion of structure-from-motion and GPS using constrained bundle adjustments," *IEEE Trans. Pattern Anal. Mach. Intell.*, vol. 34, no. 12, pp. 2489–2495, Dec. 2012.

[9] D. Larnaout, S. Bourgeois, V. Gay-Bellile, and M. Dhome, "Towards bundle adjustment with GIS constraints for online geo-localization of a vehicle in urban center," in *Proc. Int. Conf. on 3D Imaging, Modeling, Processing, Visualization & Transmission (3DIMPVT)*, Zurich, Switzerland, Oct. 2012.

[10] P. Fua, "Using model-driven bundle-adjustment to model heads from raw video sequences," in *Proc. Int. Conf. Comput. Vis. (ICCV)*, Kerkyra, Greece, Sep. 1999.

[11] P. Ozog, M. Johnson-Roberson, and R. M. Eustice, "Mapping underwater ship hulls using a model-assisted bundle adjustment framework," *Robotics and Autonomous Systems*, vol. 87, pp. 329–347, Jan. 2017.

[12] G. Gallego and A. Yezzi, "A compact formula for the derivative of a 3-d rotation in exponential coordinates," *Journal of Mathematical Imaging and Vision*, vol. 51, pp. 378–384, Mar. 2015.

[13] E. K. P. Chong and S. H. Zak, *An Introduction to Optimization*, Wiley, 2013.

[14] Q. Demoulin, F. Lefebvre-Albaret, A. Basarab, D. Kouamé, and J.-Y. Tourneret, "Derivatives calculation for constrained bundle adjustment," Tech. Rep., University of Toulouse, Feb. 2020, available at: https://www.irit.fr/~Adrian.Basarab/img/tec_derivatives.pdf.

[15] Agisoft LLC, St. Petersburg, Russia, *Agisoft Metashape User Manual: Professional Edition, Version 1.6*, 2020, available at: https://www.agisoft.com/downloads/user-manuals/.

[16] P. Virtanen and al., "SciPy 1.0: Fundamental Algorithms for Scientific Computing in Python," *Nature Methods*, 2020.

[17] *CloudCompare Version 2.6.1 user manual*, 2015, GPL software available at: http://www.cloudcompare.org/.